An image-based approach to determine the kinetics of polyQ aggregation in the neurons of *C.elegans*

Vera van Schijndel
MCLS master student
6091326

Under supervision of T. Sinnige

Sinnigelab, Membrane Biochemistry & Biophysics, Bijvoet Center for Biomolecular Research, Department of Chemistry, Faculty of Science, Utrecht University

Abstract

Protein aggregation is a pathological hallmark of a wide range of neurodegenerative diseases. The aggregation processes at molecular level have been extensively studied *in vitro*. However, The mechanism of protein aggregation *in vivo* is less established. Kinetic *in vivo* studies have been performed using the model organism *Caenorhabditis elegans.* Fluorescently labelled polyglutamine (polyQ) expressed in body wall muscle cells of living *C.elegans* aggregates into small inclusions which can be easily visualized using fluorescence microscopy. In this study, we take advantage of this model to determine the kinetics of polyQ aggregation in the neurons. We provide a novel image-based approach to quantitatively analyse the number of aggregates over time. Our results show that inclusions can be visualized and characterized using fluorescence confocal imaging in living *C.elegans* expressing pan-neuronal polyQ. Furthermore, the formation of inclusions is time, concentration and length dependent. One striking observation in this study was that only a subset of neurons contained aggregates. This study improves our understanding of aggregation mechanisms in the neurons of a living organism which is a great contribution to research focused on understanding human diseases.

Introduction

Protein aggregation is a phenomenon in which mis-folded proteins aggregate into insoluble amyloid fibrils. The toxicity of the processes associated with these fibrils is a key factor that promotes several neurodegenerative diseases[1]. So far, neurodegenerative diseases are considered to be incurable and affect millions of people worldwide[2].

In this study, we focus on protein aggregation caused by proteins containing a polyglutamine (CAG) expansion. More than 60 human proteins contain polyQ sequences[3]. Several diseases are characterized by these aggregates; most infamously Huntington's disease. Wild type huntingtin contains a trinucleotide expansion of 6-34 glutamines in the exon 1 and is not pathogenic. However, a stretch of more than 36 glutamines results in neurodegeneration[4]. It is important to clarify how proteins transform into an amyloid state in living organisms. Studying the kinetics of the processes that lead to amyloid formation reveals the molecular mechanism and rate constants involved in this process.

The mechanism of polyQ aggregation *in vitro* is extensively studied. Circular dichroism experiments showed that monomeric polyQ peptides are in a thermodynamically favoured random coil state. Clusters of monomers subsequently transform into a cross-B structure characteristic of amyloid fibrils. Once a nucleus is formed, fibril growth proceeds rapidly by the addition of monomers or oligomers[5,6]. Sigmoidal kinetics are frequently observed using Thioflavin T (ThT), a small molecule that gives strong fluorescence upon binding to amyloids[7]. Amyloid formation is caused by specific processes, including primary nucleation responsible for the initial formation of aggregates, followed by fibril elongation through the addition of precursor species[1,8]. Secondary processes are able to increase the aggregation rate to accelerate as the reaction progresses. Such mechanisms include fragmentation, in which amyloid fibrils break into smaller pieces, and secondary nucleation, in which new nuclei form from already existing amyloid fibrils[5]. *In vitro* studies showed that secondary nucleation plays a key role in polyQ aggregation[8].

The conditions *in vivo* are far from the conditions in a test tube, so it is important to study protein aggregation in intact cells. Molecular chaperones generally prevent aggregation in living cells by refolding mis-folded proteins or dissociating protein aggregates. Larger aggregates and insoluble inclusions can be removed by autophagy and lysosomal degradation. The failure of cells to maintain proteostasis contributes to the toxic effects of protein aggregates[9].

The nematode *Caenorhabditis elegans* is a powerful tool to study a large variety of biological processes *in vivo*. *C.elegans* has a relatively short lifespan of approximately 3 weeks which makes this organism very easy to study neurodegenerative disorders, since most of them are related to aging. Furthermore, *C. elegans* is transparent which makes it beneficial to study processes using *in vivo* fluorescence markers [10,11] . *C.elegans* has been used to study aggregation

processes in different tissues. PolyQ aggregation in the body wall muscle cells and neurons of *C.elegans* is length-dependent and the pathological threshold of >40Q repeats is conserved among these tissues. Furthermore, the solid nature of the inclusions in living *C.elegans* can be confirmed using FRAP and FRET experiments[12,13]. The 95 body wall muscle cells are equivalents of the vertebrate skeletal muscles. Protein aggregation kinetics are easy to analyse in body wall muscle cells because these cells are identical to each other and they are relatively large, so they can be assessed by multiple microscopy techniques[14]. *In vivo* kinetic studies showed that polyQ aggregation in body wall muscle cells is governed by stochastic nucleation in individual cells Mathematical modelling was used to determine the aggregation mechanism *in vivo*[15].

As indicated before, polyQ aggregation is a pathological hallmark of several neurodegenerative disorders, Therefore we focus in this study on the mechanism of protein aggregation in the neurons. The nervous system is the most complex organ of *C.elegans*. It consist of 302 simple, mostly unbranched neurons which can be divided into 118 anatomically different neuron classes[10]. The pharyngeal nervous system consist of 20 neurons which is independent from the somatic nervous system[16]. *C.elegans* has 68 sensory neurons which are mainly located in the head, whereby axons make connections with interneurons in the nerve ring. These sensory neurons are responsible for sensing for example chemicals, oxygen, carbon dioxide and temperature [17,18]. Motor neurons are mainly located only in body with their cell bodies on the ventral side, and they are responsible for the locomotion of *C.elegans* [10,19].

It has so far been a challenge to determine the aggregation kinetics of polyQ in the neurons, because these cells are very small and non-identical. In this research, we present an image-based workflow for unbiased inclusion counting in the neurons that enables us to perform quantitative kinetic analysis.

Materials and methods.

C. elegans methods and strains

Nematodes were maintained on nematode growth media (NGM) seeded with *Escherichia coli* OP50 at 20°C using standard methods[20]. Age-synchronized populations of *C. elegans* were generated by allowing ~10 adult animals to lay eggs on NGM plates for a period of 1-2 h. For long-term experiments, animals were transferred daily to fresh NGM plates.

Strains used in this study:

N2

AM49, rmIs172 [F25B3.3p::Q19::CFP][21]

AM47, rmIs167 [F25B3.3p::Q40::CFP][21]

AM44, rmIs190 [F25B3.3p::Q67::CFP][21]

AM52, rmIs182 [F25B3.3p::Q0::YFP] [13]

AM101, rmIs110 [F25B3.3p::Q40::YFP][13]

AM1228-31, rmIs404 [unc-54p::Q40::YFP][15]

HA659, rtIs11 [osm-10p::GFP+osm10p::HtnQ150+dpy-20(+)][17]

OH7193, otIs181 [dat-1::mCherry + ttx-3::mCherry][22]

Fluorescence imaging of inclusions

A drop of 2.5% agarose solution was deposited onto a glass slide to create a pad. 10uL of 25mM NaN_3 in M9 buffer (3 g/L KH2PO4, 6 g/L Na2HPO4, 0.5 g/L NaCl, 1mM MgSO4) was placed on the pad. ~20 worms were picked and placed in the NaN_3 droplet. A cover slip was placed on top of the pad containing the worms. Widefield imaging was performed using a Nikon Eclipse Ni-U microscope equipped with a Nikon DS-Qi2 Mono Digital Microscope Camera. Inclusions were counted manually. Images were obtained using Plan Apo Lambda 60x N.A. 1.40 oil, Plan Fluor 40x N.A. 1.30 oil, Plan Fluor 20x N.A. 0.75 oil objectives. Spinning disk confocal imaging was performed using a Plan Apo VC 60x objective with 15-30% of a 488 nm/50 mW laser on a Nikon Eclipse Ti-U. For semi-automated inclusions counting, the obtained z-stacks were thresholded in the open source imaging platform ImageJ/FIJI[23] and the inclusions were classified using the '3D objects counter' function.

Identifying aggregates using FRAP

Fluorescence recovery after photobleaching was performed on strains AM52 and AM101 on the 8th day of adulthood. Spinning disk confocal imaging was performed using a Plan Apo VC 60x objective with 4.5% of a 488 nm/150 mW laser on a Nikon Eclipse Ti with Perfect Focus System and 300 frames of 100 ms were recorded. Bleaching was performed using 10 iterations with 100% of the laser. The FRAP movies were aligned using the Template Matching plugin in ImageJ. The FRAP zone was identified as the region of interest and a control zone was selected outside of the FRAP zone. The Relative fluorescence intensity was calculated using the following equation: (fluorescence FRAP zone after photobleaching / fluorescence control zone after photobleaching) – (fluorescence FRAP zone before photobleaching / fluorescence control zone before photobleaching)[24]

Quantification protein concentrations

For strains N2, AM52, AM101, AM716 and AM1230, a total of 30 animals were picked into 16 µL M9 buffer. The samples were snap frozen in a dry ice-ethanol bath and stored at -80˚C until further processing. 4 µl 5x SDS Sample Buffer (62.5 mM Tris-HCl pH 6.8, 20% glycerol, 2% SDS, 5% beta-mercaptoethanol, 0.1% bromophenol blue) was added to each sample. The samples were incubated at 95 ˚C for 15 minutes and the total volumes were loaded onto SDS PAGE gels. Recombinant EYFP (RayBiotech) was used to determine the amounts of protein in each lane. The western blots were probed with JL-8 anti-GFP primary antibody and IRDye 800 CW secondary antibody and scanned using LI-COR Odyssey infrared imaging system.

The volume of neurons was determined from fluorescent images using the Voxel Counter plugin in ImageJ. The total fluorescence intensity per animal was divided by the number of neurons.

High throughput imaging of aggregation kinetics in *C.elegans*

20 age-synchronized worms of strains AM1228, AM1229, AM1230, AM1231 and AM101 were picked in a 384-well plate containing 100 µL M9 buffer (3 g/L KH2PO4, 6 g/L Na2HPO4, 0.5 g/L NaCl, 1mM MgSO4)) containing 25 mM NaN3 as an anaesthetic. Widefield and confocal imaging was performed using a high content screening system (Yokogawa CellVoyager). Fluorescent signal was detected using a 488 nm laser. A 10x objective was used to visualise polyQ aggregates in body wall muscle cells and a 20x objective was used to visualise polyQ aggregates in neurons.

Stitching of the acquired images was performed using the Grid/Collection Stitching[25] plugin in ImageJ. Inclusions counting was done using a custom made pipeline in Cellprofiler[26]. This pipeline uses the brightfield images to identify the worms and the fluorescence images to identify the inclusions. The output file contains the number of inclusions per worm.

Results

Inclusions can be visualized using fluorescence microscopy

PolyQ proteins tagged with a fluorescent protein form intracellular inclusions when expressed in the neurons of *C.elegans*[13]. We used worm strains expressing different polyglutamine proteins tagged with CFP or YFP under the control of the promotor for F25B3.3 to see whether we could visualise the polyQ inclusions that are formed in the neurons of *C.elegans.* The gene product of the F25B3.3 promotor is RasGRP, a guanyl nucleotide-releasing protein for Ras, which is expressed throughout the nervous system of *C.elegans*[27].

Inclusions were observed in animals expressing Q40-CFP and Q67-CFP using widefield microscopy, whereas in worms expressing Q19-CFP only diffuse polyglutamine was observed (*figure S1A*). This observation corresponds to the length-dependent threshold of >Q40 for the formation of bright polyQ inclusions[13]. Q19-CFP, Q40-CFP and Q67-CFP inclusions were counted manually using an epifluorescence microscope. Worms expressing Q67-CFP in the neurons showed more inclusions as the worm ages until a plateau of around 20 inclusions was reached on day 4. Q40-CFP inclusions appeared after day five of adulthood (*figure S1B*). We experienced that the fluorophore expressed in these worm strains bleached very quickly which made it difficult to count inclusions and thus determine the kinetics using widefield microscopy.

To monitor polyQ aggregation kinetics, we focused on animals expressing Q0-YFP and Q40-YFP in the neurons. The worms were visualised using spinning disk confocal microscopy. We observed bright inclusions in the neurons of Q40-YFP animals, but not in the neurons of animals expressing Q0-YFP. The Q40-YFP inclusions appeared in different shapes and sizes *(figure 1A)*, whereas Q40-YFP inclusions in body wall muscle cells of *C.elegans* have been observed to be uniform in shape and size. This is likely caused by the difference in morphology between the body wall muscle cells and neurons. Furthermore, polyQ inclusions appeared in both cell bodies and neuronal processes, suggesting polyQ aggregation is not limited to a specific area in the neurons. Some neurons acquired multiple inclusions *(figure1A, third image)*, possibly caused by fragmentation processes.

To confirm that the bright inclusions are caused by protein aggregation, we used Fluorescence recovery after photobleaching (FRAP). FRAP is a suitable technique to assess the aggregation state of different polyQ proteins *in vivo*. Experiments on animals that express diffuse Q0-YFP, showed recovery after photobleaching *(figure 1B,D)*, indicating soluble protein expressed in these neurons. The bright spots in Q40-YFP neurons showed no recovery after photobleaching, indicating that the Q40 inclusions are insoluble because of the formation of polyQ aggregates. *(figure 1C,D)*. These observations are consistent with FRAP experiments carried out previously in living *C.elegans*[12,13]. The inclusions observed using spinning disk confocal microscopy in Q40-YFP animals can thus be defined as polyQ aggregates.

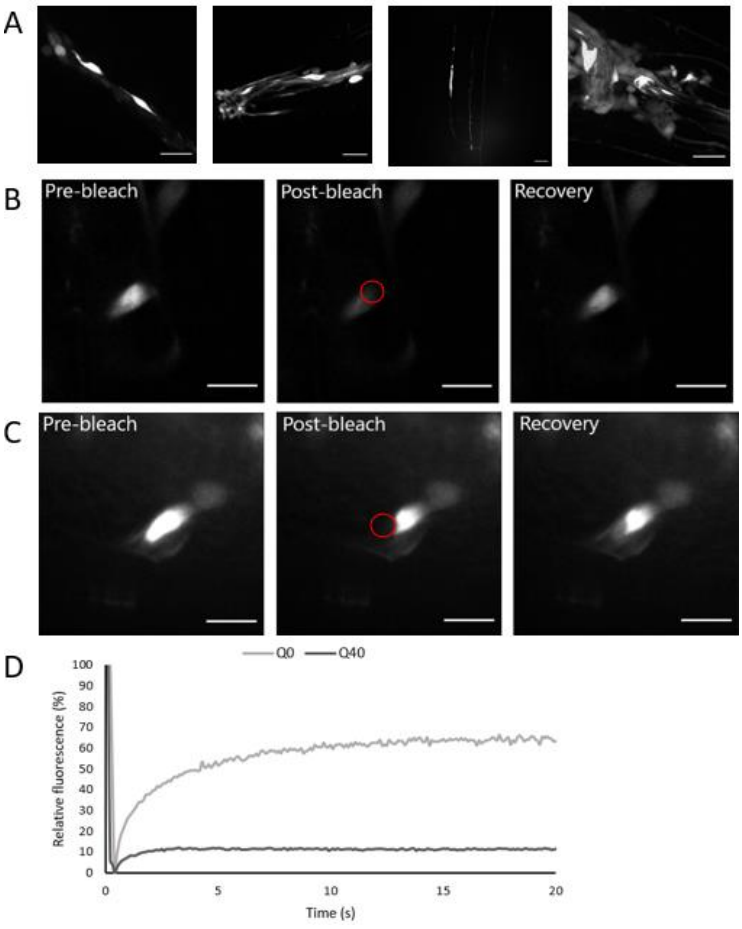

Figure 1. Inclusions can be confirmed using FRAP. (A) Confocal images of Q40-YFP animals showing bright inclusions in the neurons. Scale bar: 10µm. (B,D) FRAP in *C.elegans* neurons expressing Q0-

YFP. The photobleached area (circle) recovers rapidly, indicating soluble proteins. Scale bar: 5 µm. (C,D) FRAP in *C.elegans* neurons expressing Q40-YFP. The photobleached area (circle) does not recover which is consistent with aggregation. Scale bar: 5 µm. (D) Quantification of the signal intensity.

Quantitative analysis of aggregation kinetics in *C.elegans*

In vitro kinetic studies have provided a good mechanistic understanding of protein aggregation at the molecular level[5,6,8]. Moreover, an *in vivo* kinetic model for polyQ aggregation in the body wall muscle cells of living *C.elegans* was recently presented[15]. However, aggregation kinetics in the neurons of *C.elegans* have not been established before. To monitor polyQ aggregation, the head region of age-synchronized Q40-YFP and Q0-YFP worms were imaged daily from day one till day seven of adulthood using confocal spinning disk microscopy. The head region was imaged because the distribution of inclusions can easily be visualized here. This region contains distinct neuronal processes and the nerve ring can also be identified[28]. A diffuse fluorescence intensity was observed in the Q0-YFP control strain. Inclusions in Q40-YFP worms were already observed on the first day of adulthood and increased over time *(figure 2A).*

We employed semi-automated image analysis to count inclusions over time. The number of inclusions counted using this method is comparable with the numbers yielded by manual counting (*figure s2)*. However, semiautomated inclusion counting is unbiased and more quantitative. The number of inclusions increased over time until a plateau is reached of around 11 inclusions on day five of adulthood *(figure 2B)*. The plateau does not correspond to the total number of about 180 neurons in the head region. This reveals that only a subset of neurons contain polyQ aggregates, suggesting that these neurons are more susceptible to aggregation.

Previous research showed that inclusion formation in body wall muscle cells is concentration dependent[15]. We compared homozygous with heterozygous Q40-YFP animals to investigate if this is also holds for polyQ aggregation in the neurons. Heterozygous animals have 50% less gene copies than homozygous animals. Slower, but similar kinetics were observed in heterozygous animals and the number of inclusions in these worms reached a plateau value of around seven inclusions on day five of adulthood *(figure 2B).* Based on these observations, inclusion formation in the neurons depends on the polyQ concentration.

The intracellular protein concentration in the neurons was quantified from Western blot analysis *(figure s3)*. Using the average volume of the total amount of neurons, which is about 15 pL, an intracellular concentration of about 3,45 mM was calculated for Q40-YFP worms. The intracellular concentration of worms expressing Q40-YFP in body wall muscle cells was calculated to be 1.34 mM. The nucleation rate is concentration dependent, so it is expected that the nucleation rate of Q40-YFP aggregation in the neurons is faster compared to Q40-YFP aggregation in body wall muscle cells. However, we observed a similar kinetic curve for aggregation in neurons as previously observed in body wall muscle cells[15]. This indicates that neurons are less susceptible to Q40-YFP aggregation than body wall muscle cells.

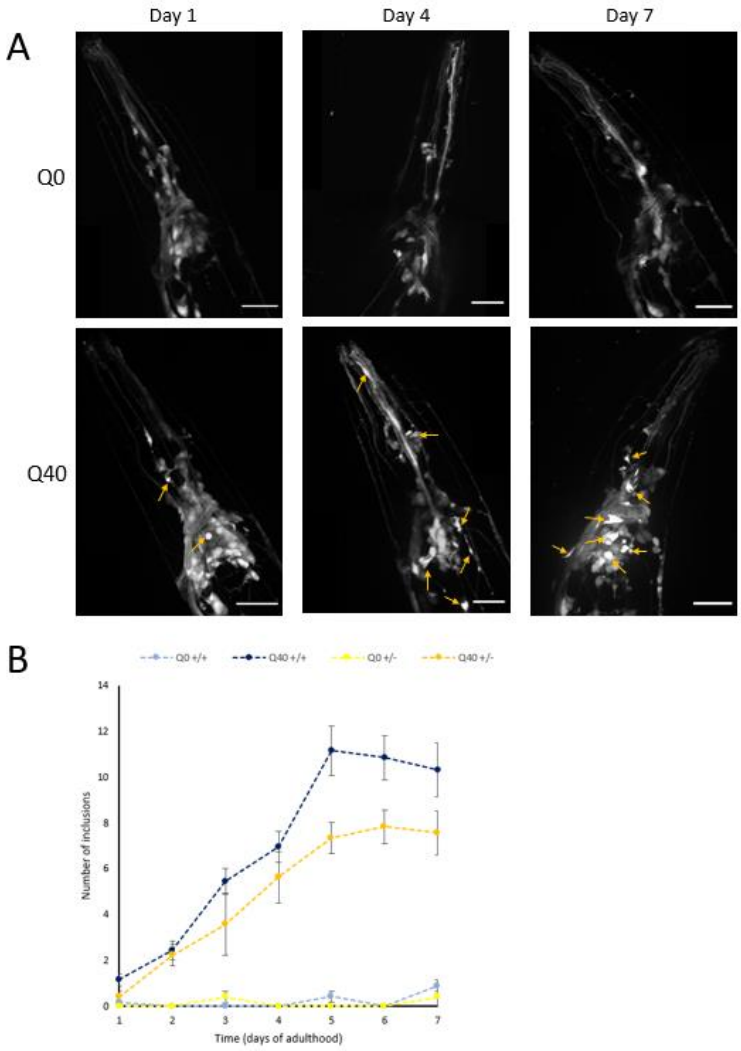

Figure 2. Inclusion formation of YFP tagged polyQ proteins in the *C.elegans* neurons over time. (A) Confocal images of Q40-YFP animals showing bright inclusions in the neurons on day 1, 4 and 7 of adulthood. A diffuse fluorescence intensity was observed in the Q0-YFP control strain. Scale bar: 20µm. (B) Average number of inclusions in the head neurons of homozygous (+/+) and heterozygous (+/-) worms expressing Q0-YFP and Q40-YFP on day 1-7 of adulthood. Error bars indicate the SEM. *n*=15-20 worms for each strain and timepoint.

All neurons are susceptible to aggregation of a longer polyQ stretch

Protein aggregation in animals that contain pan-neuronal expression of polyQ proteins is length-dependent[13]. Animals expressing a higher polyQ expansion generally contain more aggregates than animals expressing a lower polyQ length. Confocal images showed that Q67-YFP protein was localized to discrete inclusions in the neurons of *C.elegans (figure 3A)*. This is different from the diffuse distribution that was observed in Q0-YFP and Q40-YFP worms.

Semi-automatic inclusion counting revealed a total of around 200 inclusions in the head region of Q67-YFP worms *(figure 3B)*. This number of aggregates corresponds to the total number of neurons in the head region suggesting each neuron contains one or two inclusions. These results show that all neurons, independent of subtype, are susceptible to the formation of Q67-YFP inclusions. This can be explained by the fact that Q67-YFP proteins are more aggregation prone than Q40-YFP proteins.

Dopaminergic neurons do not show polyQ aggregation

The previous observation that only a subset of neurons in worms expressing Q40-YFP contain inclusions, raised the question which neurons are included in this subset. To check whether dopaminergic neurons are a part of this subset, we crossed worms expressing the fluorophore mCherry in dopaminergic neurons with worms expressing Q40-YFP. Confocal images showed no correlation between Q40-YFP aggregates and dopaminergic neurons, suggesting that there is no polyQ aggregation in dopaminergic neurons *(figure 4)*.

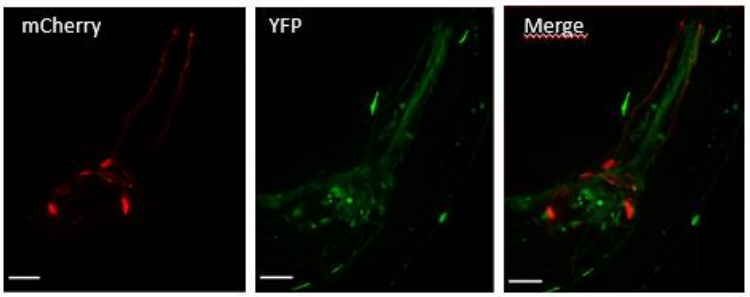

Figure 4. No polyQ aggregation in dopaminergic neurons (A) Confocal images of Q40-YFP animals expressing mCherry in dopaminergic neurons and pan-neuronal Q40-YFP. Merging the images shows no correlation between the inclusions and dopaminergic neurons. Scale bar: 20µm.

High throughput imaging and automated inclusion counting in *C.elegans* using Cellprofiler

We have provided a good understanding of inclusion formation in the neurons of *C.elegans.* However, to monitor protein aggregation kinetics *in vivo* more efficiently, we used a high throughput imaging platform combined with a dedicated analysis platform in Cellprofiler. This pipeline is able to identify the individual worms using brightfield images and identify the inclusions using fluorescence images *(figure S4)*. The output provided us the number of inclusions per worm. This workflow has been tested already using several images obtained using the CellVoyager microscope and has been shown to be an applicable tool for automated inclusion counting in *C.elegans.*

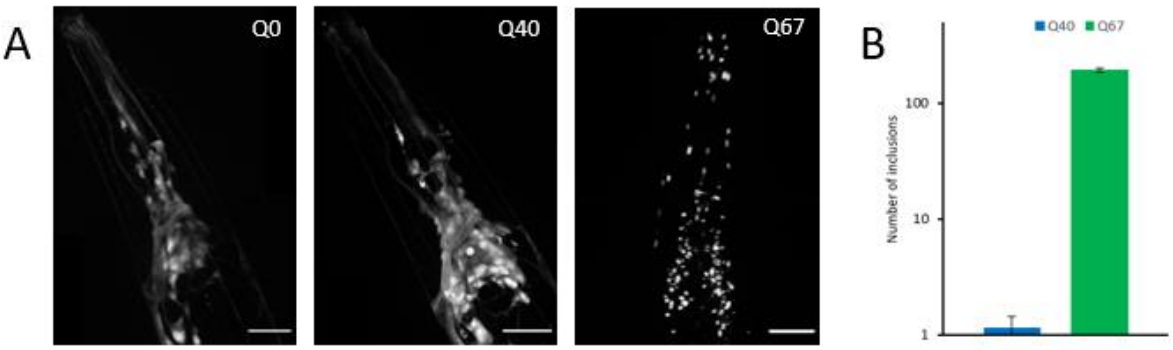

Figure 3. Inclusion formation is polyQ length dependent (A) Confocal images of Q0-YFP, Q40-YFP, Q67-YFP animals on day 1 of adulthood. Only diffuse signal is observed for Q0-YFP worms, 1 or two inclusions are observed for Q40-YFP worms and alle neurons contain inclusions in Q67-YFP worms. Scale bar: 20µm. (B) Average number of inclusions in the head neurons of worms expressing Q40-YFP and Q67-YFP on day 1 of adulthood. n=20; error bars indicate the SEM.

Discussion

In this study, we showed that polyQ aggregates can be visualized using fluorescence confocal spinning disk imaging *(figure 1A, 2A)*. Spinning disk confocal microscopy is suitable for imaging *C.elegans*, because it enabled us to acquire z-stack images through the worms of ca. 80 um in diameter in a few of seconds. Furthermore, individual aggregates can be distinguished using this technique. Manual inclusion counting can be achieved using widefield microscopy by moving the stage in the z-direction. However, Semi-automated inclusion counting cannot be applied on widefield images, since the inclusions of only one plane of the relatively thick worm can be visualized in focus, while the majority of the inclusions is out of focus *(figure S1A)*. Q40-YFP aggregates appeared in cell bodies and neuronal processes in different shapes and sizes, whereas inclusions in body wall muscle cells are uniform in shape and size[12,15]. This difference is likely caused by the morphological properties of the neurons compared with the body wall muscle cells of *C.elegans*

We used fluorescent recovery after photobleaching (FRAP) to confirm that the bright inclusions in Q40-YFP animals that were observed using spinning disk confocal microscopy are polyQ aggregates *(figure 1B)*. FRAP has previously shown to be a suitable technique for monitoring the biophysical properties of polyQ proteins in living *C.elegans*[12,13]. We observed a difference between the state of aggregation of Q40-YFP compared to Q0-YFP. Diffuse Q0-YFP exhibited around 65% recovery of the fluorescence signal after photobleaching, while previous experiments showed around 100% recovery of the same protein[13]. This is most likely caused by overall bleaching of the fluorophore over time throughout the head region of the worm.

Semi-automated inclusion counting was used to monitor polyQ aggregation in the neurons of living *C.elegans (figure 2A,2B)*. Semi-automated inclusion counting is preferred over manual inclusions, because this technique is more quantitative and unbiased. Using this method, we were able to determine the kinetics of polyQ aggregation in the neurons. The kinetic curve of polyQ aggregation in the neurons is similar to the kinetic curves determined for aggregation in body wall muscle cells, suggesting stochastic nucleation in individual cells[15]. Q40-YFP aggregation in the neurons showed a significant dependence on protein concentration (*figure 2B).* The nucleation rate is dependent on the intracellular protein concentration. The polyQ concentration was higher for the strain expressing Q40-YFP in the neurons than for the worms expressing Q40-YFP in body wall muscle cells[15]. Therefore, we expected faster kinetics of polyQ in the neurons. This was however not the case, so we concluded that neurons are less susceptible to polyQ aggregation than body wall muscle cells.

A big difference between polyQ expression in the pan-neuronal models used in this research and the body-wall muscle cell models described in previous studies is that Q40-YFP aggregates in a cell-specific way in the neurons, whereas Q40 aggregation in the neurons is stochastic. That not all neurons contain aggregates is consistent with previous studies reporting only a fraction of 20-30% of the neurons in patient material contain inclusions[29]. It is difficult to conclude which neurons belong to the fraction that are more susceptible to polyQ aggregation using pan-neuronal expressed polyQ proteins. Studies have shown that GABAergic neurons are most susceptible to huntingtins disease in the human brain[30]. Dopaminergic neurons did not appear to contain any polyQ aggregates in *C.elegans (figure 4)*. Human dopaminergic neurons are most affected by protein aggregation in Parkinson's disease[31]. To determine which neurons contain polyQ inclusions, future experiments will be carried out using worm models expressing polyQ in distinct neurons.

Previous studies have shown that polyQ aggregation is length dependent[32]. Q67-YFP proteins aggregate more rapidly than Q40-YFP proteins in living *C.elegans*[12,13]. We observed that neurons resistant to Q40-YFP aggregation, are susceptible to the more aggregation prone Q67 protein. Furthermore, we observed exclusively discrete foci in the neurons of Q67-YFP suggesting that there is no more diffuse protein expressed in these worms. These worms are not suitable for determining the kinetics, since a plateau value of around 200 inclusions is already reached on day 1 of adulthood.

We generated a workflow which includes high throughput imaging of polyQ aggregation in living *C.elegans* combined with a custom made image-analysis pipeline in Cellprofiler *(figure S4)*. Spinning disk confocal imaging of a multi-well plate enables us to image several strains in parallel. Furthermore, automated inclusions is preferred above manual counting because it is fast and unbiased. Cellprofiler is an excellent tool for high throughput imaging analysis because it has the ability to process large datasets by building a reproducible analysis pipeline. The kinetics of protein aggregation have yet to be determined using this technique, but we envisage that this technique will yield us new insights into protein aggregation in a living animal.

In conclusion we provided a novel image-based technique to monitor inclusion formation in the neurons of living *C.elegans* using semi-automated inclusion counting. Like in body wall muscle cells, protein aggregation is concentration, time and length-dependent. However, we observed that Q40-YFP aggregation only occurs in a minor fraction of neurons. These findings improved our understanding of aggregation mechanisms in the neurons of a living organism which is a great contribution to research focused on understanding human diseases.

Acknowledgement

We thank the Morimoto lab for most of the strains used in this study. Some strains were provided by the CGC, which is funded by NIH Office of Research Infrastructure Programs (P40 OD010440). We thank the Biology Imaging Center (BIC) of Utrecht University to provide access, support and training in the microscopy techniques that were used.

Literature

1. Knowles, T. P. J., Vendruscolo, M. & Dobson, C. M. The amyloid state and its association with protein misfolding diseases. *Nat. Rev. Mol. Cell Biol.* **15**, 384–396 (2014).
2. Hebert, L. E., Scherr, P. A., Bienias, J. L., Bennett, D. A. & Evans, D. A. Alzheimer disease in the US population: Prevalence estimates using the 2000 census. *Arch. Neurol.* **60**, 1119–1122 (2003).
3. Schaefer, M. H., Wanker, E. E. & Andrade-Navarro, M. A. Evolution and function of CAG/polyglutamine repeats in protein-protein interaction networks. *Nucleic Acids Res.* **40**, 4273–4287 (2012).
4. Zoghbi, H. Y. & Orr, H. T. G Lutamine R Epeats and. *Annu. Rev. Neurosci.* **23**, 217–247 (2000).
5. Chiti, F. & Dobson, C. M. Protein misfolding, amyloid formation, and human disease: A summary of progress over the last decade. *Annu. Rev. Biochem.* **86**, 27–68 (2017).
6. Chen, S., Berthelier, V., Yang, W. & Wetzel, R. Polyglutamine aggregation behavior in vitro supports a recruitment mechanism of cytotoxicity. *J. Mol. Biol.* **311**, 173–182 (2001).
7. Xue, C., Lin, T. Y., Chang, D. & Guo, Z. Thioflavin T as an amyloid dye: Fibril quantification, optimal concentration and effect on aggregation. *R. Soc. Open Sci.* **4**, (2017).
8. Kakkar, V. *et al.* The S/T-Rich Motif in the DNAJB6 Chaperone Delays Polyglutamine Aggregation and the Onset of Disease in a Mouse Model. *Mol. Cell* **62**, 272–283 (2016).
9. Hipp, M. S., Park, S. H. & Hartl, U. U. Proteostasis impairment in protein-misfolding and -aggregation diseases. *Trends Cell Biol.* **24**, 506–514 (2014).
10. Corsi, A. K., Wightman, B. & Chalfie, M. A Transparent window into biology: A primer on Caenorhabditis elegans. *WormBook* 1–31 (2015) doi:10.1895/wormbook.1.177.1.
11. Kaletta, T. & Hengartner, M. O. Finding function in novel targets: C. elegans as a model organism. *Nat. Rev. Drug Discov.* **5**, 387–399 (2006).
12. Morley, J. F., Brignull, H. R., Weyers, J. J. & Morimoto, R. I. The threshold for polyglutamine-expansion protein aggregation and cellular toxicity is dynamic and influenced by aging in Caenorhabditis elegans. *Proc. Natl. Acad. Sci. U. S. A.* **99**, 10417–10422 (2002).
13. Brignull, H. R., Moore, F. E., Tang, S. J. & Morimoto, R. I. Polyglutamine proteins at the pathogenic threshold display neuron-specific aggregation in a pan-neuronal Caenorhabditis elegans model. *J. Neurosci.* **26**, 7597–7606 (2006).
14. Gieseler Kathrin, Qadota Hiroshi, B. G. M. Development, structure, and maintenance of C. elegans body wall muscle. *Wormb. Online Rev. C. elegans Biol.*
15. Sinnige, T. *et al.* Kinetic analysis reveals that independent nucleation events determine the progression of polyglutamine aggregation in C. elegans. *Proc. Natl. Acad. Sci. U. S. A.* **118**, (2021).
16. Avery, L. & Horvitzt, H. R. Pharyngeal pumping continues after laser killing of the pharyngeal nervous system of C. elegans. *Neuron* **3**, 473–485 (1989).
17. Faber, P. W., Alter, J. R., Macdonald, M. E. & Hart, A. C. Polyglutamine-mediated dysfunction and apoptotic death of a Caenorhabditis elegans sensory neuron. *Proc. Natl. Acad. Sci. U. S. A.* **96**, 179–184 (1999).
18. Bretscher AJ, Kodama-Namba E, B. K. Temperature, oxygen, and salt-sensing neurons in C. elegans are carbon dioxide sensors that control avoidance behavior. *Neuron* **69**, 1099–1113 (2011).
19. Mcintire, S. L., Jorgensen, E. M., Kaplan, J. M. & Horvitz, H. R. The GABAergic Nervous System of C. elegans. *Nature* **364**, 337–341 (1993).
20. Brenner, S. THE GENETICS OF CAENORHABDITIS ELEGANS. *Genetics* **77**, 71 LP – 94 (1974).
21. Gidalevitz, T., Ben-Zvi, A., Ho, K. H., Brignull, H. R. & Morimoto, R. I. Progressive Disruption of Cellular Protein Folding in Models of Polyglutamine Diseases. *Science (80-.).* **311**, 1471–1475 (2006).
22. Flames, N. & Hobert, O. Gene regulatory logic of dopamine neuron differentiation. *Nature* **458**, 885–889 (2009).
23. Schindelin, J. *et al.* Fiji: an open-source platform for biological-image analysis. *Nat. Methods* **9**, 676–682 (2012).
24. Phair, R. D. & Misteli, T. High mobility of proteins in the mammalian cell nucleus. *Nature* **404**, 604–609 (2000).
25. Preibisch, S., Saalfeld, S. & Tomancak, P. Globally optimal stitching of tiled 3D microscopic image acquisitions. *Bioinformatics* **25**, 1463–1465 (2009).
26. Jones, T. R. *et al.* CellProfiler Analyst: data exploration and analysis software for complex image-based screens. *BMC Bioinformatics* **9**, 482 (2008).
27. Ebinu, J. O. *et al.* RasGRP, a Ras guanyl nucleotide-releasing protein with calcium- and diacylglycerol-binding motifs. *Science (80-.).* **280**, 1082–1086 (1998).
28. Chalfie, M. *et al.* The neural circuit for touch sensitivity in Caenorhabditis elegans. *J. Neurosci.* **5**, 956–964 (1985).
29. DiFiglia, M. *et al.* Aggregation of huntingtin in neuronal intranuclear inclusions and dystrophic neurites in brain. *Science (80-.).* **277**, 1990–1993 (1997).
30. Jeon, I. *et al.* Neuronal properties, in vivo effects, and pathology of a Huntington's disease patient-derived induced pluripotent stem cells. *Stem Cells* **30**, 2054–2062 (2012).
31. Hirsch, E. C., Graybiel, A. M. & Agid, Y. Melanized dopaminergic neurons are differentially affected in Parkinson's disease. *Nature* **334**, 345--348. (1988).
32. Scherzinger, E. *et al.* Self-assembly of polyglutamine-containing huntingtin fragments into amyloid-like

fibrils: Implications for Huntington's disease pathology. *Proc. Natl. Acad. Sci. U. S. A.* **96**, 4604–4609 (1999).
33. Macdonald, D. *et al.* Quantification assays for total and polyglutamine-expanded huntingtin proteins. *PLoS One* **9**, (2014).

Supplementary

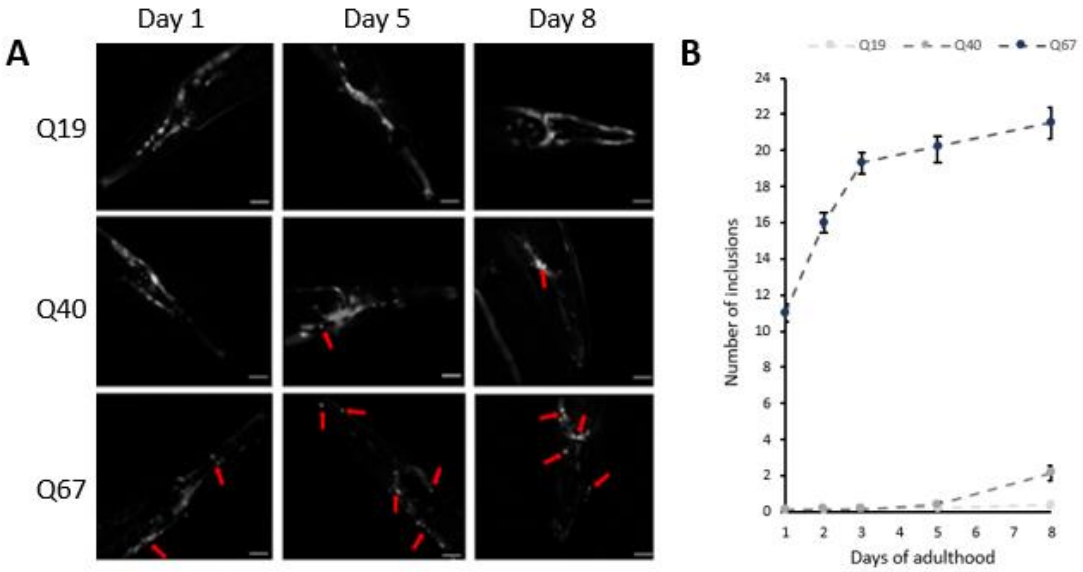

Figure S1. PolyQ-CFP expressed in *C.elegans* neurons. (A) Widefield images of *C.elegans* strains AM49, AM47 and AM44. Strains expressing Q19-CFP only show soluble polyglutamine, whereas Q40-CFP and Q67-CFP display bright inclusions in the head neurons (red arrows). Scale bar: 20µm. (B) Average number of inclusions per worm over time for age-synchronized populations of *C.elegans* expressing polyQ-CFP in the neurons. Error bars indicate the SEM. n=20 animals per strain and timepoint.

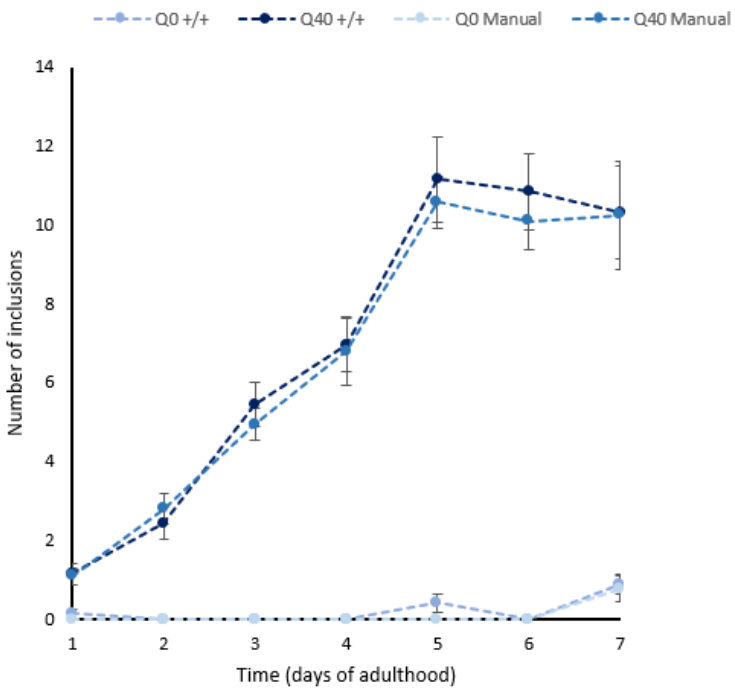

Figure S2. Semi-automated inclusion counting versus manual inclusion counting in worms expressing Q0-YFP and Q40-YFP over time. Error bars indicate the SEM. *n*= 15-20 worms per strain and timepoint.

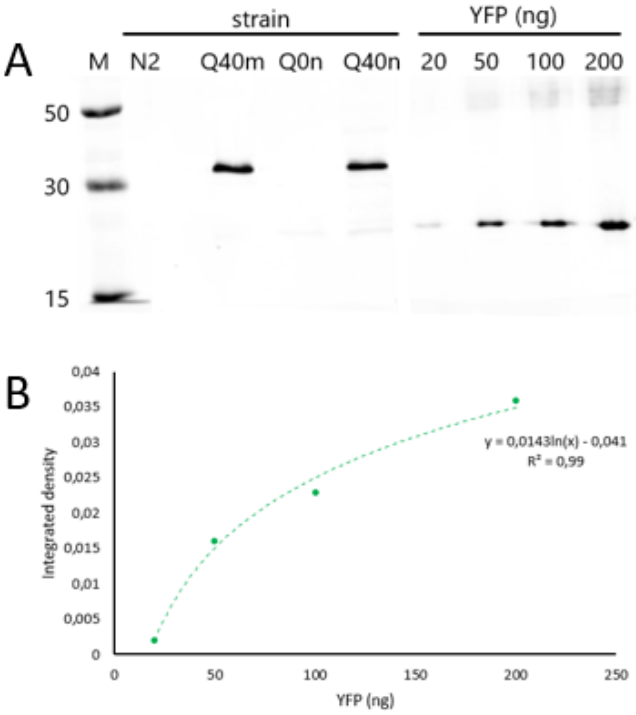

Figure S3. Determination of Q40-YFP concentration expressed in body wall muscle cells and neurons. (A) Western blot with worm lysates of 30 animals on the first day of adulthood and recombinant YFP. (B) Calibration curve of the integrated density of YFP bands. The function was used to calculate the amount of Q40-YFP in the worms.

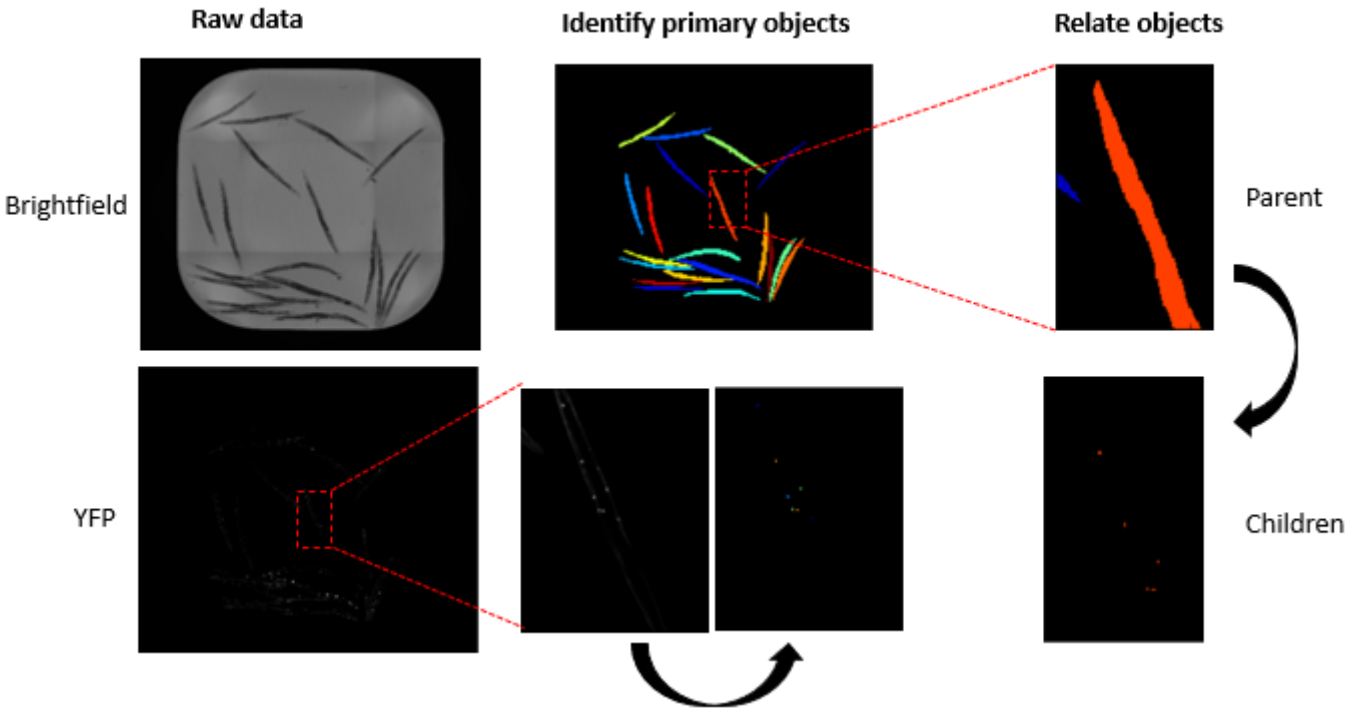

Figure S4. High thoughput image-based quantification of inclusions in *Celegans*. Brightfield and Fluorescence images were obtained using the Cellvoyager microscope. Using a custom made pipeline in cellprofiler, worms were identified using brightfield images, and inclusions were identified using fluorescence images.

Layman's abstract

A wide range of neurodegenerative diseases, most notably Alzheimer's disease, are caused by specific proteins that clump together in the brain resulting in protein aggregates. Neurodegenerative diseases are considered to be incurable because there is no known way to reverse neuronal degeneration. Medications are available to temporarily improve or slow progression of the symptoms. The risk of being affected by one of these diseases increases with age. There is a critical need to find new therapeutics for neurodegenerative diseases. Therefore we need to improve our understanding of the molecular mechanism of protein aggregation. One type of proteins that are known to form aggregates are proteins that contain a polyglutamine repeat (polyQ). Several diseases are characterized by polyQ proteins, most infamously Huntington's disease. PolyQ aggregation is length-dependent and has a pathological threshold of 40 glutamine repeats (Q40).

Test tube experiments have provided a great progress in understanding the process of amyloid formation. However, he mechanism of amyloid formation in a multicellular organism is less established. The tiny roundworm *Caenorhabditis elegans* is a very suitable model organism to study neurodegenerative diseases. A model for polyQ aggregation the muscle cells of living *C.elegans* was recently presented. The mechanism of polyQ aggregation in the neurons is however poorly understood. Studying protein aggregation in the neurons comes with a few challenges. Neurons are much smaller compared to muscle cells the nervous system contains many different types of cells.

To overcome these challenges, we used worms that contain polyQ proteins tagged with a fluorophore in the neurons. The fluorophore enables us to monitor aggregation of polyQ proteins in living *C.elegans* using light microscopy. We observed bright spots in the neurons of *C.elegans* containing fluorescently labelled Q40. We did not observe this in worms expressing fluorescently labelled Q0 in the neurons. We identified these bright spots as aggregates using a technique called Fluorescent recovery after photobleaching (FRAP). In order to understand the mechanism of protein aggregation, we have to monitor aggregate formation over time. We imaged Q0 and Q40 worms daily using spinning disk confocal microscopy and subsequently counted the number of inclusions using a software. We found that the number of polyQ aggregation in the neurons depended on time, concentration and length. Strikingly, we observed that most neurons did not contain any aggregates, suggesting that these neurons were resistant to Q40 aggregation. This study enabled us to improve our current understanding of the aggregation mechanism in the neurons of a living organism. This is a great contribution to future research focused on understanding human diseases.